Available online at www.sciencedirect.com
SCIENCE DIRECT®
Journal of Sound and Vibration 284 (2005) 103–132
JOURNAL OF SOUND AND VIBRATION
www.elsevier.com/locate/jsvi

The excitation of ground vibration by rail traffic: theory of vehicle–track–soil interaction and measurements on high-speed lines

L. Auersch*

Bundesanstalt für Materialforschung und –prüfung (BAM), D 12200 Berlin, Germany

Received 16 September 2002; received in revised form 14 April 2004; accepted 8 June 2004
Available online 18 November 2004

Abstract

This article presents an integrated model for the computation of vehicle–track interaction and the ground vibrations of passing trains. A combined finite element and boundary element method is used to calculate the dynamic compliance of the track on realistic soil whereas multi-body models are used for the vehicle. The dynamic stiffness of the vehicle and that of the track are combined to calculate the dynamic axle loads due to the irregularities of the vehicle and the track as well as those due to sleeper passing excitation. These loads serve as input for the calculation of ground vibration near railway lines in the time and frequency domains.

The theoretical methods and results have been proven by experiments in several respects and at several instances. First, on the occasion of the test and record runs of the Intercity Experimental, there was a very good quality of the vehicle and of the newly built track so that the *deterministic* parts of the excitation—the static load and the sleeper-passing component—could clearly be identified, the first being of minor importance apart from the track. Second, simultaneous measurements of the vehicle, the track and the soil at three different track situations were performed where we could verify the different parts of the *stochastic* excitation and their importance for the ground vibrations. The irregularities of the vehicle are dominant at high frequencies whereas the irregularities of the track are more important at lower frequencies. The comparison of the theory and the measurements also points to the phenomena of the vehicle–track resonance and the scattering of the quasi-static axle impulses by randomly varying soil.

*Tel.: +49 30 8104 3290; fax: +49 30 8104 1727.
E-mail address: lutz.auersch-saworski@bam.de (L. Auersch).

0022-460X/$ - see front matter © 2004 Elsevier Ltd. All rights reserved.
doi:10.1016/j.jsv.2004.06.017

Nomenclature

a	half-width of the track
a^*	normalized half-width of the track
a_A	axle spacing
a_C	length of a carriage
d	sleeper spacing
$\mathrm{d}f$	a difference of frequencies
D	damping ratio
E	modulus of elasticity
EI	flexural stiffness (of the rail)
f	frequency
f_S	sleeper-passage frequency
F_T	flexibility of the track
G	shear modulus (of the soil)
i	index (summation, iteration)
j	imaginary unit
k_P	pad stiffness
K	dynamic stiffness of the vehicle and the track (constant part)
K_V	dynamic stiffness of the vehicle
K_T	dynamic stiffness of the track
K_{T0}	static stiffness of the track
K_1	time-varying part of the dynamic stiffness
m_W	mass of the wheel
p	force
p_V	vehicle force
p_T	track force
p_0	static axle load
p_1	dynamic axle load due to sleeper passage
r	radius, distance of observation point
r^*	normalised radius
r_W	radius of the wheel
s	irregularities (of the vehicle s_V or the track s_T)
t	time (of excitation)
t'	arrival time
T	delay time
u	displacement
u_V	displacement of the vehicle
u_T	displacement of the track
u_0	displacement due to the static load (starting point of iteration)
u_1	displacement due to sleeper passage
u_{10}	displacement due to static sleeper passage
v_S	shear wave velocity of the soil
v_T	train speed
X	spectrum of axle sequence
x	distance from the track
y	point of excitation measured along the track
λ	wavelength of the irregularity
ν	the Poissons' ratio
ρ	mass density
ρA	mass per length of the rail
ω	circular frequency

1. Introduction

Ground vibration near railway lines has been a research and consulting subject of the Federal Institute for Materials Research and Testing (BAM) for more than two decades. To this end, a number of measurements have been made (Fig. 1) and different theoretical models have been developed. As pointed out by a number of authors [1–3] and shown in a previous contribution [4], the amplitudes and frequencies of the ground vibration are strongly influenced by the soil. The present contribution focuses on the excitation process of the railway vibration.

Here, the excitation is expressed as the static and dynamic forces between the wheels and the rail. The excitation can be of a deterministic nature, such as the static axle loads and the sleeper-passing component, or of a stochastic nature, such as the irregularities of the track and the irregularities of the vehicle (out-of-round wheels). The frequencies considered range

from 0 to 150 Hz while ground vibration near railway lines in the range of 4–100 Hz are primarily of interest. Often a clear distinction can be found between the low-frequency ($f<30$ Hz) and the high-frequency part of the vibration, and these parts may be partially correlated with the stochastic excitation by the track (the low-frequency part) and the vehicle (the high-frequency part).This contribution intends to cover all the types of excitation which are of importance.

In the literature, another distinction is made between the quasi-static and the dynamic part of the excitation according to the absence or presence of inertial effects of the vehicle [2]. In Refs. [5,6] the quasi-static method is used to analyse the effects of the moving static load over a track with sleepers. The strongest effect in these studies is the (quasi-static) sleeper-passage effect. However, the sleeper passage results in an important dynamic load due to the variation of the track stiffness on and between the sleepers [7,8], which should be included in the analysis, too. In Ref. [9], the quasi-static method was compared with high-speed measurements similar to those in Ref. [10], indicating only a moderate agreement.

Another type of excitation, which is also due to the passage of static loads, was first presented in Ref. [11], namely, the scattering of the axle-impulses by a randomly varying soil. Both measurements presented here give further evidence of this. In addition, it is clearly shown that the deterministic static part is negligible, as it rapidly diminishes with distance from the railway line.

To analyse the stochastic dynamic part of the ground vibration, it is necessary to obtain some experimental information about the irregularities of the vehicle and the track by measurements on the vehicle [12] or on the track [2], and it is necessary to solve the vehicle–track interaction problem.

Recently, a number of methods have been developed to calculate the moving load effects on the track and on the soil [13–16]. For the special case of a "critical train speed"—that is, a train speed close to the wave speed of the soil—an amplification is predicted regarding especially the displacements of the track. The special effects of moving loads may be even more pronounced in combination with a layered soil with its resonance and cut-off frequencies [3,13]. For the situation discussed in this contribution and for most real situations, this effect is not of interest. More literature about railway vibration and about layered soil is given in Ref. [4].

This contribution consists of three main parts: (i) the theoretical solution, (ii) the experimental results of the ICE test runs on the new track (Fig. 1) and (iii) the simultaneous measurements of vehicle, track and surrounding soil. First, the theoretical models of each subsystem—vehicle, track and soil—are presented and then the solution of their interaction is discussed.

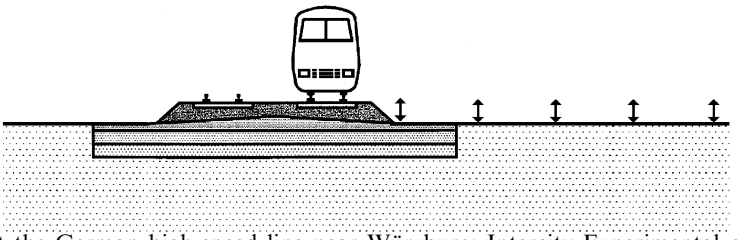

Fig. 1. The test situation at the German high-speed line near Würzburg: Intercity Experimental on ballasted track, measurement of ground vibration at 2.5–100 m from the track.

In Section 2.2., the vehicle–track resonance and the irregularities of vehicle and track are studied. The effects of the sleeper passage are derived in Sections 2.3, and in Section 2.4 the effects of moving static (and dynamic) loads are presented. For each type of excitation there are corresponding experimental results: the deterministic loads are proved in Section 3 (high-speed measurements) and the stochastic components—the irregularities of the vehicle and the track—are analysed in Section 4 (simultaneous measurements). In addition in Sections 3 and 4, a stochastic component due to the soil is discussed in context with the measured mid-frequency ground vibration.

2. Theory on the interaction of vehicle, track and soil

2.1. Methods and parameters of the sub-systems

For each sub-system—vehicle, track and soil—an appropriate method of calculation is used (Fig. 2). Starting with the base, the *soil* is described by dynamic point-load solutions which are calculated by a frequency–wavenumber approach [4]. The point-load solutions of a homogeneous or layered soil are used to calculate the wavefield caused by a passing train or—in other words—the ground vibrations near railway lines. But the same point-load solutions are also used to calculate the track behaviour. They are introduced in a boundary element algorithm to yield a stiffness-matrix of the soil, which is coupled with a finite element matrix of the track or any other structure. In this way, the interaction of the soil with ballasted and slab tracks as well as buildings with the soil can all be calculated [17].

The track–soil system of Fig. 3 is investigated for a harmonic wheelset load or, in other words, for a pair of harmonic wheel loads. The compliance of the *track* under this wheelset load is calculated as a function of frequency. A ballasted track with a UIC60 rail, stiff rail pads ($k_P = 300\,\mathrm{kN/mm}$) and concrete sleepers according to the detailed list of parameters given in Appendix A is analysed. In Fig. 4, the amplitude and the phase of the compliance or flexibility function $F_T(f)$ are presented for four different homogeneous soils. The flexibility of the ballasted track is strongly influenced by the stiffness of the soil, especially at low frequencies. In addition, the ballasted track on homogeneous soil has a strong damping due to the radiation into the interior of the soil, which can be identified by the high phase of the flexibility function. In Fig. 5, some additional results of a slab track are presented, which are used for the discussion of the simultaneous measurements in Section 4. Compared to the ballasted track, the damping of a slab track is reduced considerably by the elastic rail pads ($k_P = 80\,\mathrm{kN/mm}$). More details on different tracks on different homogeneous or layered soils are given in Refs. [18,19].

The mixed boundary-element finite-element models of the track–soil systems consist of 2×40 rail elements, 11×12 sleeper elements, $44 \times 12 \times 2$ volume elements of the ballast and a fully coupled soil element of $45 \times 13 \times 3$ degrees of freedom. For the calculation of vehicle–track interaction, these complex track–soil models are represented only by their results—their dynamic track compliances $F_T(f)$. This may be called a sort of substructure method.

Various models can be used for the railway *vehicle*, for example, the four-mass model consisting of two wheels, bogie and half of a car-body used in Ref. [7]. We require the dynamic stiffness $K_V(f)$ as a function of frequency. In general, this is a matrix which returns the dynamic wheel

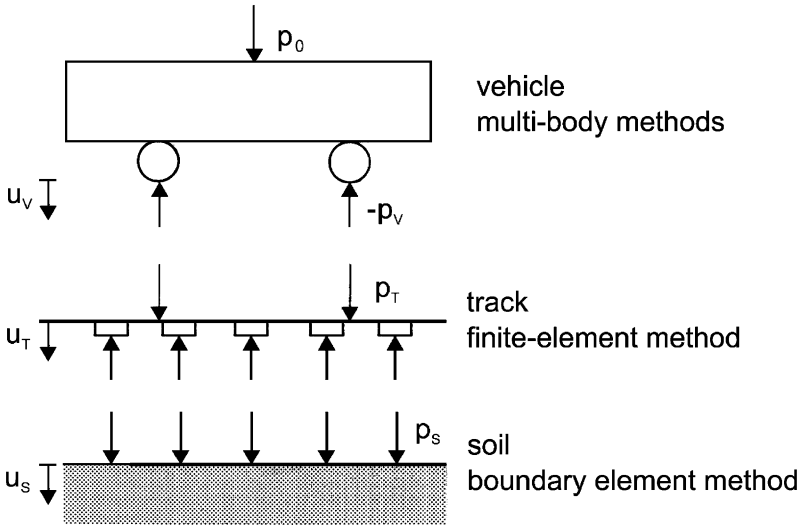

Fig. 2. The interaction of the vehicle, the track and the soil—coupling of different methods for each sub-system.

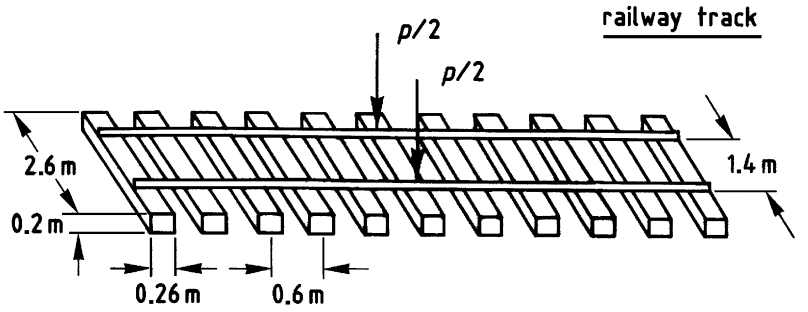

Fig. 3. The dimensions of the track in theory and experiment.

loads p_V caused by the displacements u_V of the wheels. The dynamic stiffness of the vehicle represents the inertial effects and the eigenfrequencies of the vehicle such as the vertical eigenfrequency of the carriage and the vertical and the rotational eigenfrequencies of the bogie. Instead of restricting the model to rigid masses, vehicles with elastic components can also be included, as in Ref. [12] for example. However, the effects of elasticity are not particularly strong, and taking rigid masses seems to be a conservative approach. For specific purposes and at sufficiently high frequencies, it was found that the simplest model of a rigid wheelset of mass m_W would give reasonable results, too. In this case, we have the dynamic vehicle stiffness

$$K_V = -\omega^2 m_W, \tag{1}$$

which can be introduced most easily in the vehicle–track interaction presented in the next section.

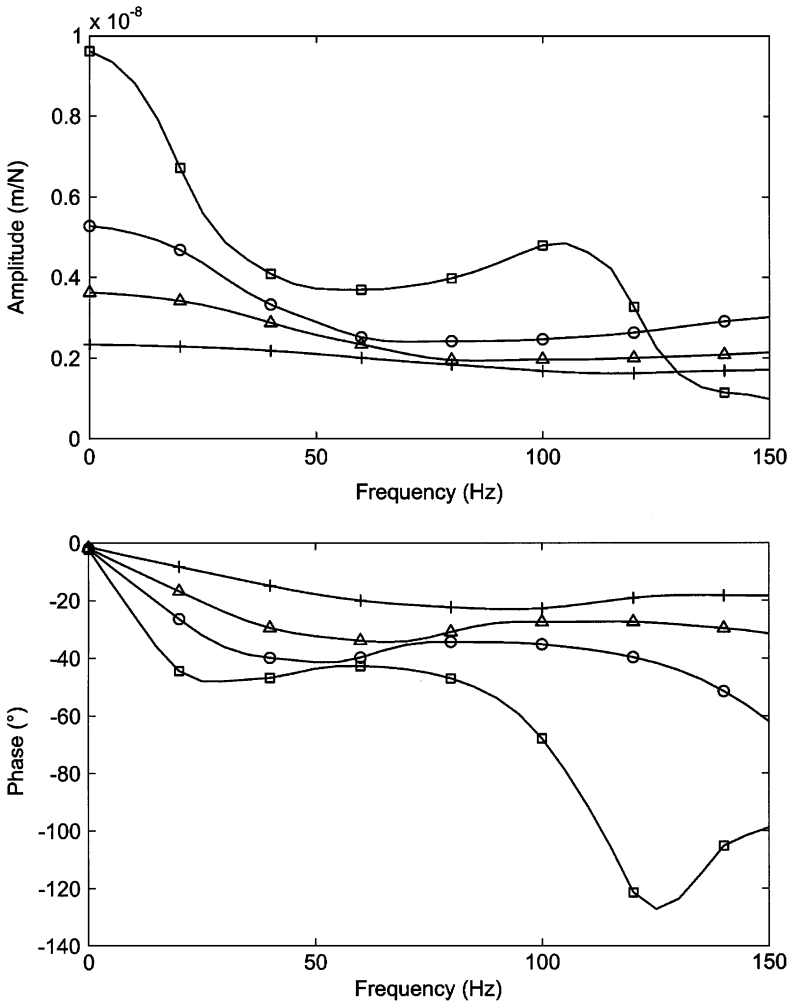

Fig. 4. The dynamic compliance of a ballasted track on different homogeneous soils with $v_S = 100\,\mathrm{m/s}$ □, 150 m/s ○, 200 m/s △, 300 m/s +.

2.2. Dynamic axle loads due to irregularities of the vehicle and the track

The sub-systems for vehicle and for track–soil must be coupled to calculate the dynamic axle loads. A description is used in which only the forces p_V and p_T and the displacements u_V and u_T of the contact points of the vehicle and the track are used. The vehicle is described by its dynamic stiffness K_V

$$p_V = K_V u_V, \tag{2}$$

where p_V and u_V are spectra and K_V is a transfer function.

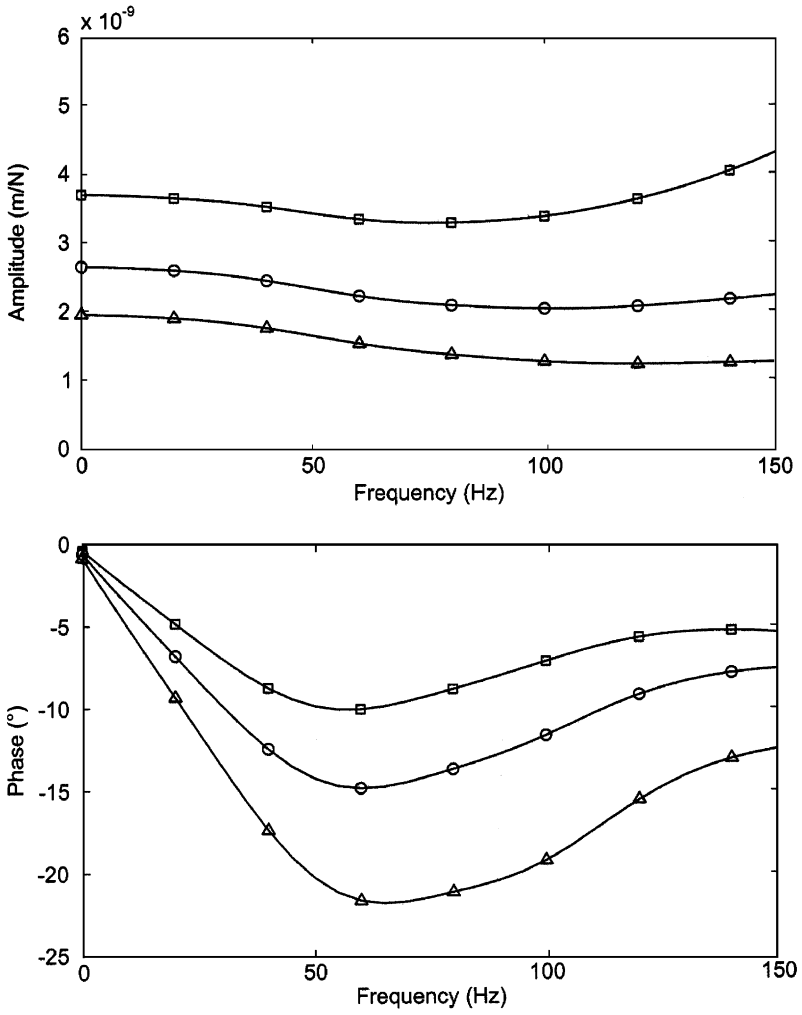

Fig. 5. The dynamic compliance of a slab track with different rail pads $k_P = 80\,\mathrm{kN/mm}$ □, 150 kN/mm ○ and 300 kN/mm △.

The track is described by its compliance F_T

$$u_T = F_T p_T. \tag{3}$$

Although, we need the track compliance for a moving load, we use the compliance for a fixed load as presented in the preceding section. This is acceptable because the difference between moving and fixed load is small, if the speed of the train is smaller than the wave speed of the soil

$$v_T < v_S \tag{4}$$

(see for example Refs. [11,13–16]). Instead of the compliance F_T, the stiffness $K_T = F_T^{-1}$ is used

$$p_T = K_T u_T. \tag{5}$$

To combine the vehicle and the track, the following two equations are used: The force p_T acting on the track and the force p_V acting on the vehicle (the wheelset) are the same except for the sign (see Fig. 2)

$$-p_T = p_V. \tag{6}$$

The displacement u_V of the wheelset differs from the displacement u_T of the track by the amount of the irregularity s

$$u_V = u_T + s, \tag{7}$$

where s can be any irregularity of the track, of the surface of the rail or the out-of-round of the wheel. By eliminating the track displacement u_T and the vehicle force p_V in Eqs. (2),(5)–(7), we get the system equation

$$(K_V + K_T)u_V = K_T s, \tag{8}$$

which yields the vehicle response u_V due to the irregularities s

$$u_V = (K_V + K_T)^{-1} K_T s, \tag{9}$$

and the corresponding interaction force (by using Eqs. (5) and (6))

$$p_T = -p_V = -K_V u_V = -K_V (K_V + K_T)^{-1} K_T s. \tag{10}$$

The train speed v_T is introduced into the calculation by determining the frequency

$$f = v_T/\lambda \tag{11}$$

together with the wavelength λ of a harmonic irregularity.

Fig. 6 shows the transfer function u_V/s of Eq. (9) for the ballasted track considered in Section 2.1 with the rigid wheelset of mass $m_W = 1500$ kg. The transfer function starts at the value 1, increases to a maximum at the vehicle–track eigenfrequency and decreases for high frequencies. The vehicle–track eigenfrequency depends strongly on the stiffness of the soil, varying from 50 to 100 Hz. The vehicle–track resonance is considerably stronger for a slab track with soft rail pads (Fig. 7). For a slab track, the stiffness of the rail pads is the most important parameter in determining the vehicle–track eigenfrequency.

2.3. Dynamic axle loads due to sleeper passage

2.3.1. A general method for a system with time-varying stiffness

In the case of a discretely supported rail, the track stiffness K_T depends on the position of the load between or on the sleepers. For a train running with speed v_T, this means a periodical variation of the track stiffness with the sleeper-passage frequency

$$f_S = v_T/d, \tag{12}$$

where d is the sleeper distance. The system equation (8) is

$$[K_V + K_T + K_1(t)]u_V = p \tag{13}$$

with the time-varying part $K_1(t)$ of the track stiffness and a load p where the most important load—the static load—is considered in the next section. K_T and K_V are read as operators which

act on time functions u_V and p. An approximate solution of the system equation (13) is given in a general form in this section. A special solution for practical railway problems is given in the next section and a simpler derivation of this special version is presented in Appendix B.

We start at the general system equation

$$[K + K_1(t)]u = p. \tag{13'}$$

If $K_1(t)$ is small compared to the stiffness K, we have the following iterative method for the time-varying system. At first, we calculate the solution

$$u_0 = K^{-1}p \tag{14}$$

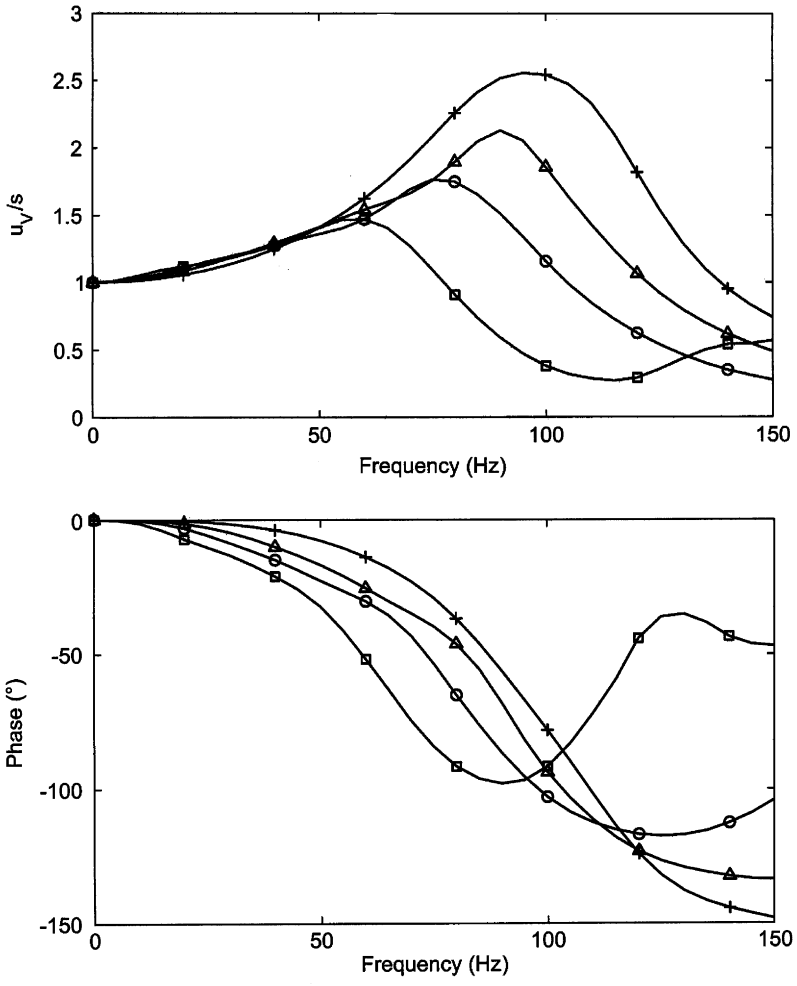

Fig. 6. The transfer function of vehicle–track interaction for the ballasted tracks on different homogeneous soils with $v_S = 100$ m/s □, 150 m/s ○, 200 m/s △, 300 m/s +.

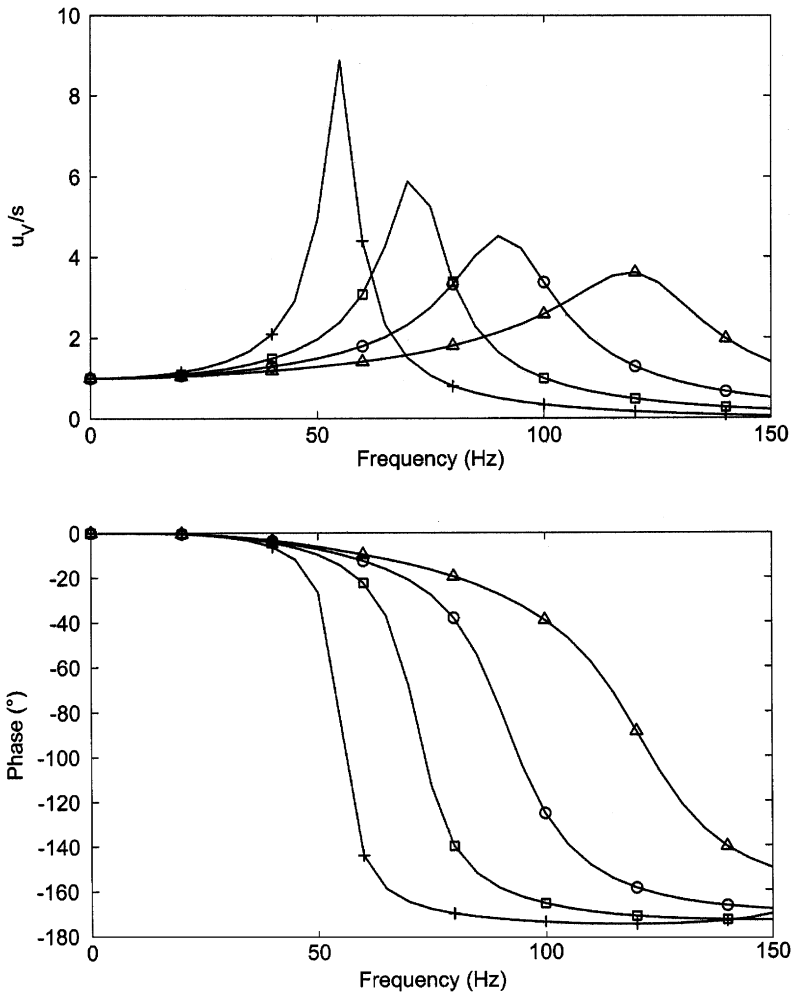

Fig. 7. The transfer function of vehicle–track interaction for a slab track with different rail pads $k_P = 40\,\mathrm{kN/mm}$ +, 80 kN/mm □, 150 kN/mm ○, 300 kN/mm △.

as if there is no time-varying stiffness. When u_0 is introduced in the complete system equation (13′), we get an error

$$[K + K_1(t)]u_0 = p + K_1(t)u_0. \tag{15}$$

The error $K_1(t)\,u_0$ is taken as a new excitation and again the solution u_1 of the time-independent problem is calculated

$$u_1 = -K^{-1}K_1(t)u_0 = -K^{-1}K_1(t)K^{-1}p. \tag{16}$$

Again we get a small error when u_1 is introduced in the complete system equation. We can continue this procedure and we get a series of equations

$$u_i = -K^{-1}K_1(t)u_{i-1}. \tag{17}$$

By summing these equations for $i = 0, \ldots, n$, we get the approximate solution

$$u = \sum_{i=0}^{n} u_i = K^{-1}\left(p - K_1(t)\sum_{i=0}^{n-1} u_i\right), \tag{18}$$

which fulfils the system equation (13′) with a small error (by rearrangement of Eq. (18))

$$[K + K_1(t)]\sum_{i=0}^{n} u_i = p + K_1(t)u_n. \tag{19}$$

If only the first two Eqs. (14) and (16) of the procedure are used, we can write

$$u_1 = -K^{-1}K_1(t)u_0 = -K^{-1}K_1(t)K^{-1}p \tag{20}$$

for the additional displacement u_1 due to the variation K_1 of the stiffness, and for the additional dynamic axle-load p_1 we have (using Eqs. (5) and (6))

$$p_1 = -K_V u_1 = K_V K^{-1}K_1(t)K^{-1}p. \tag{21}$$

These approximate solutions (20) and (21) are further reduced by specifying the variation of the stiffness due to the sleeper passage.

2.3.2. The passage of static loads over a track with equally spaced sleepers

In particular, with the dominating static load p_0 of the train instead of p, we get a solution in the frequency domain. The stiffness variation $K_1(t)$ is a periodic variation with the sleeper-passage frequency f_S (12). Moreover, it is almost exclusively a harmonic variation as the higher harmonics are negligible [8,20]. Therefore, we can rewrite Eq. (20) as

$$u_1 = -K^{-1}(f_S)K_1(0)K^{-1}(0)p_0 \tag{22}$$

and Eq. (21) as

$$p_1 = K_V(f_S)K^{-1}(f_S)K_1(0)K^{-1}(0)p_0 \tag{23}$$

by using the appropriate values of the transfer functions K, K_1 and K_V. Eqs. (22) and (23) are read from right to left as follows: as p_0 is static, we use $K^{-1}(f = 0)$. As $K^{-1}(0)p_0$ is static too, we use $K_1(f = 0)$. $K_1(0)\ K^{-1}(0)\ p_0$ is harmonic with frequency f_S, therefore, we use $K^{-1}(f_S)$. $K^{-1}(f_S)$ $K_1(0)\ K^{-1}(0)\ p_0$ in turn is harmonic and $K_V(f_S)$ is used. Eq. (23) of the sleeper-distance load consists of a frequency-dependent factor $K_V(f_S)\ K^{-1}(f_S)$ (transfer function) and a constant factor $K_1(0)\ K^{-1}(0)\ p_0$ which can be regarded as an excitation.

We can compare the sleeper-passage solution (23) with the loads due to irregularities (10) of Section 2.2. For train speed $v_T \to 0$, we get the quasi-static solution of (22)

$$u_{10} = -K^{-1}(0)K_1(0)K^{-1}(0)p_0, \tag{24}$$

and therefore we can replace the constant excitation factor by

$$-K_1(0)K^{-1}(0)p_0 = K(0)u_{10} = K_{T0}u_{10}. \tag{25}$$

The sleeper-distance load (23) can therefore be written as

$$p_1 = -K_V K^{-1} K_{T0} u_{10}, \tag{26}$$

which includes nearly the same transfer function as the load (10) due to irregularities s

$$p_T = -K_V K^{-1} K_T s,$$

where only the frequency-dependent track stiffness K_T must be replaced by the static value K_{T0}.

Results for the measuring situation described in Section 3 and Appendix A will be presented here. For a ballasted track with a rail UIC60 and sleeper distance $d = 0.6$ m, the additional (peak-to-peak) displacement of the wheel between two sleepers is $2u_{10} = 0.016$ mm (for $p_0 = 100$ kN) for a stiff track, and it decreases to $2u_{10} = 0.01$ mm for a soft track, almost independent of whether the soil or the rail pad is soft. Results for a stiff soil with a shear wave speed of $v_S = 270$ m/s and a wheelset with $m_W = 1700$ kg are given in Fig. 8 as a function of train speed. The dynamic loads due to the sleeper-passage excitation increase strongly with frequency or with speed respectively. The maximum force of $p_1 = 15$ kN is reached at the vehicle–track eigenfrequency for $v_T = 200$ km/h. At higher speeds or frequencies, the force decreases, tending to the constant asymptote of about 10 kN. This is regarded as an important conservative effect for high-speed railway traffic.

2.4. Simulation of moving loads on the ground

The propagation of waves due to the passage of a train are calculated on the basis of point-load solutions of a homogeneous or layered half-space. There are methods that work in the frequency domain where the frequency-dependent behaviour of layered soils can be clearly demonstrated [4]. Some of the results achieved in the frequency domain can be used in the approximate simulation in the time domain presented in this section. The moving loads of the train are assumed to be time harmonic loads including the static load with zero frequency.

The simplest solution for the displacements $u(r,f)$ at a distance r from a harmonic point-load p of frequency f is that of a homogeneous half-space which can be approximated by [4]

$$u(r,f) = \frac{p(1-\nu)}{2\pi G r} \mathrm{e}^{-Dr^*} \begin{cases} 1 & \text{for } r^* \leqslant 2,5, \\ \sqrt{r^*/2,5} & \text{for } r^* > 2,5, \end{cases} \tag{27}$$

where the parameters are the shear modulus G ($= 1.3 \times 10^8$ N/m^2), the Poissons' ratio ν ($= 0.3$), the material damping D ($= 5\%$), the shear-wave speed v_S ($= 270$ m/s), and

$$r^* = \omega r / v_S \tag{28}$$

is a dimensionless distance or frequency. The values in brackets are the parameters of the measuring site near Würzburg.

The forces acting on the track—for example those calculated in the preceding section—are distributed along and across the track. The simulation uses a point-load p' for each axle of the

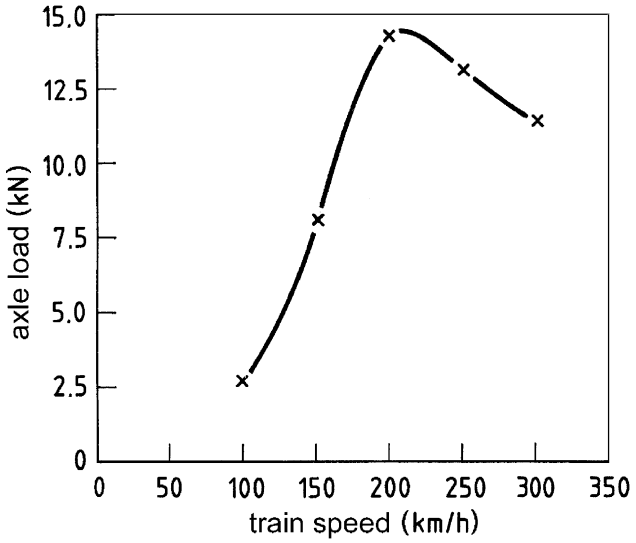

Fig. 8. The dynamic axle-load due to sleeper-passing excitation with stiffness variation $K_1/K = 5\%$.

train, which is the actual axle-load p modified according to the effect of the load distribution on the vibrations of the soil. This can be expressed by a frequency-dependent factor

$$\frac{p'}{p} = \begin{cases} \dfrac{\sin a^*}{a^*} & \text{for } a^* \leqslant \dfrac{\pi}{2}, \\ \dfrac{1}{a^*} & \text{for } a^* > \dfrac{\pi}{2}, \end{cases} \tag{29}$$

where

$$a^* = \omega a / v_S \tag{30}$$

is a frequency parameter including the half-width a of the track. This is derived by assuming a uniformly distributed load across the track width $2a$. The response of the soil to these load components has contributions with different phases and their superposition leads to a reduction of amplitudes compared to a concentrated load

$$\frac{p'}{p} = \frac{u_a}{u_0} = \frac{\int_{-a}^{+a} \mathrm{e}^{\mathrm{j}\omega x/v_S} \mathrm{d}x}{2a} = \frac{\sin \omega a/v_S}{\omega a/v_S}. \tag{31}$$

The practical prediction formula (29) uses the envelope of this theoretical result (31).

The calculated axle loads are applied to the soil for each axle of the complete train while the point of excitation moves forward with the speed of the train. For each harmonic load of each axle, a wave is propagated according to the corresponding point-load solution $u/p(r, f_i)$ of the soil

$$u(t') = \frac{u}{p}(r, f_i)\, p'(t), \tag{32}$$

where the distance r depends on the point of excitation $y_i(t)$

$$r = \sqrt{x^2 + y_i^2(t)}. \tag{33}$$

The displacement is the response at arrival time t'

$$t' = t + r/v_S, \tag{34}$$

whereas t is the loading time. Adding all components together and differentiating with respect to time leads to the particle velocity of the observation point.

There are several works [13–16] in which the effects of moving loads are studied in more detail. It has been found that there are additional effects to those presented here if the speed of the train reaches the wave speed of the soil. This situation is very seldom found in practice because the soil usually has wave speeds higher than 100 m/s. One of these rare situations was measured and presented in Ref. [4]. The soil was very soft and the observed high amplitudes are mainly due to the soft soil rather than wave speed effects. In addition, the published effects of uniform soils are certainly stronger than under realistic non-uniform soil conditions.

Figs. 9 and 10 present the results for a train consisting of two carriages and a locomotive travelling at $v_T = 200$ km/h. In Fig. 9, only the static loads are applied. The calculated soil vibrations at 2.5, 5, 10 and 20 m are quite different. Close to the track every bogie is identifiable as a pulse, whereas further away from the track the whole train is present only as a single up and downward wave. As can be seen by the scales of the vertical axes, the corresponding amplitudes decrease very rapidly with distance.

In Fig. 10, the dynamic loads are included as (i) the sleeper passing load p_1 according to the preceding section and (ii) an additional harmonic load $p_2 = 0,05p_0$ at $f = 25$ Hz. As the results are very similar to the measured ones, both are discussed together in the next section.

3. Measurements with the ICE-train

Three series of measurements were performed during the test runs of the ICE on the newly built track near Würzburg (see Fig. 1). There we have a ballasted track, as described in Section 2, on a surface line over stiff soil. The different configurations of the train are shown at the top of Fig. 14 and the train speed was varied between 100 and 300 km/h (for more details about the parameters of the measurements see Appendix A). Fig. 11 shows a result from the first measurements where the experimental train consists of a locomotive and two carriages. The components of vibration are very similar to those from the theory (Fig. 10):

A very low-frequency component is only observable close to the track, and with increasing distance this quasi-static component vanishes. There is a mid-frequency component (10–40 Hz) which is most dominant at the far-field. This is a characteristic behaviour of the soil and is attributed to the higher damping of high-frequency components. The high-frequency component (80–120 Hz) is due to the sleeper-passage excitation. The single frequency of sleeper passage is spread into a broad band when the load moves towards to and away from the observation point, as expected from the Doppler effect.

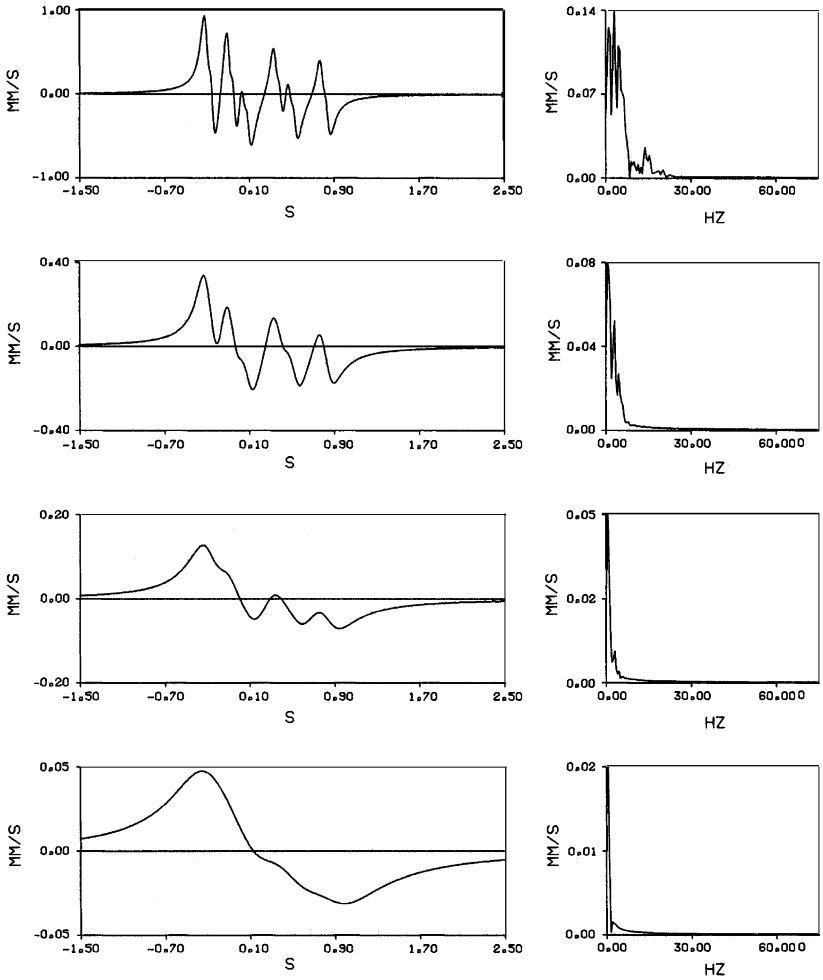

Fig. 9. Simulation of the ground vibration due to the passage of the *static loads* with $v_T = 200$ km/h. Time histories (left) and Fourier spectra (right) of the particle velocities at different distances from the railway line, $r = 2.5$, 5, 10, 20 m (from top to bottom).

The measurements as well as the calculations were performed with different train speeds. The amplitudes of the high-frequency component (the rms-value at distances of 10–15 m) are given in Fig. 12. As calculated for the sleeper passing excitation, the maximum amplitudes are found at $v_T = 200$ km/h. At this train speed, the sleeper passing frequency meets the vehicle–track eigenfrequency. For higher speeds or higher frequencies, the dynamic load no longer increases and the soil vibration even decreases due to the material damping of the soil.

Corresponding results for the mid-frequency range are shown in Fig. 13. The characteristic of this frequency range changed during the three series of measurements. During the first and third measurements a clear increase of the corresponding amplitudes was observed with increasing train speed whereas they scattered around a constant value for the second measurement. The measuring conditions changed during the three measurements. The track used and the measuring line

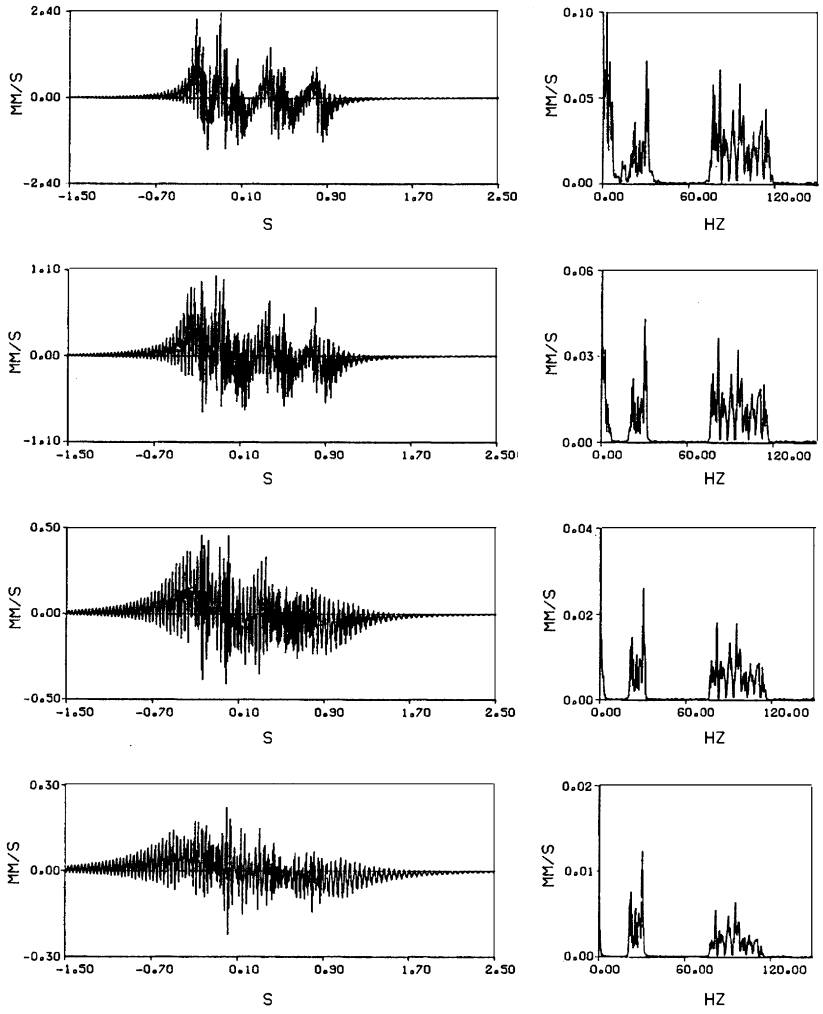

Fig. 10. Simulation of the ground vibration due to the passage of the *static and dynamic loads* with $v_T = 200$ km/h. Time histories (left) and Fourier spectra (right) of the particle velocities at different distances from the railway line, $r = 2.5$, 5, 10, 20 m (from top to bottom).

changed from east to west, and the configuration of the test train changed, too (top of Fig. 14). The mid-frequency spectra are analysed in detail by comparing them with the axle-sequence spectra of the passing train (bottom of Fig. 14). For the second measurement, a clear shift of frequencies can be seen in accordance with the speed of the train, and the shapes of the Fourier spectra agree well with that of the passing axle-loads (Fig. 15). More details on axle-sequence spectra are given in Appendix C and in Ref. [18].

The good correlation between the theoretical axle-passage spectrum and the spectra of the ground vibration leads to the conclusion that static loads are the cause of these mid-frequency vibrations. All other kinds of excitation would give a different spectrum, especially due to different phase relations between the different axles (see the arguments in Ref. [18]). As the

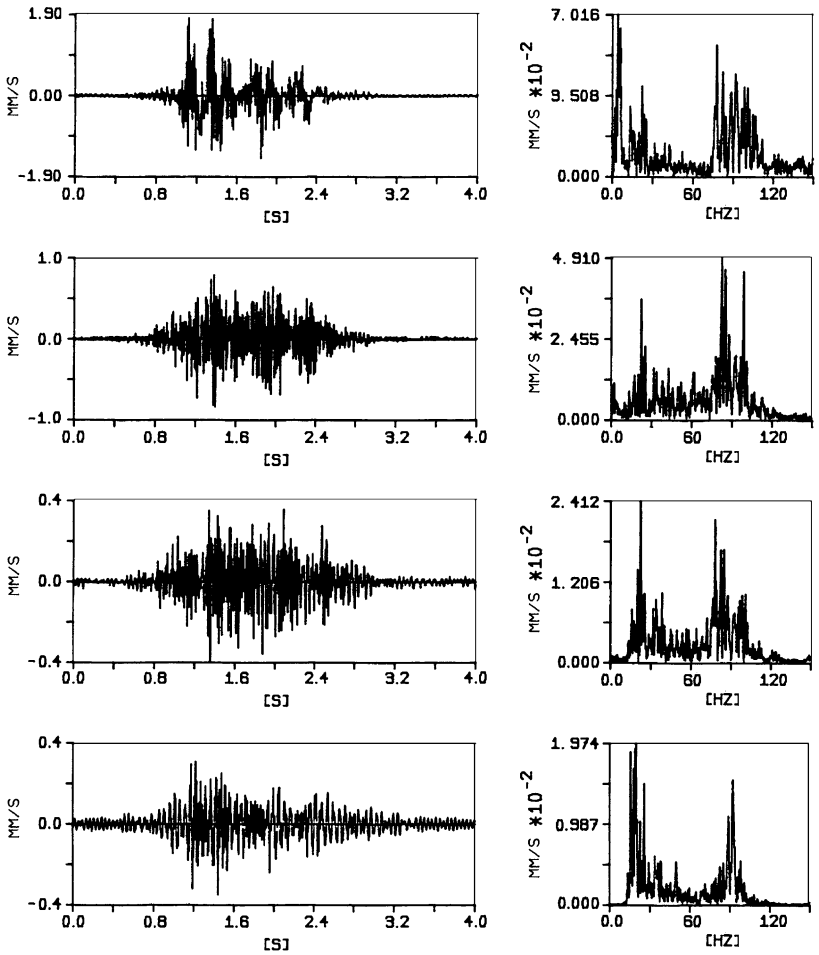

Fig. 11. *Measured ground vibration* due to the passage of the Intercity Experimental with $v_T = 200$ km/h. Time histories (left) and Fourier spectra (right) of the particle velocities at different distances from the railway line, $r = 2.5$, 5, 10, 20 m (from top to bottom).

deterministic ground vibration due to the static loads is very small, it is concluded that the measured amplitudes can only be the stochastic reaction to the static loads. This idea was first presented by Huber [11] who gave a first experimental indication and showed the considerable numerical effects of a slightly varying wave speed of the soil.

The soil reaction to each impulse of a passing axle is the same for each point, if the soil is regular, but it varies if the soil has slightly differing properties at different points. Thus in a uniform soil, the impulses at different points of excitation yield a quasi-static reaction of the soil when superposed. The superposition of the differing soil reactions in a non-uniform soil yields the mean quasi-static response but there are also irregular contributions to the soil reaction. This scattering of the axle impulses is considered as a main part of the measured train-induced ground vibrations in that case.

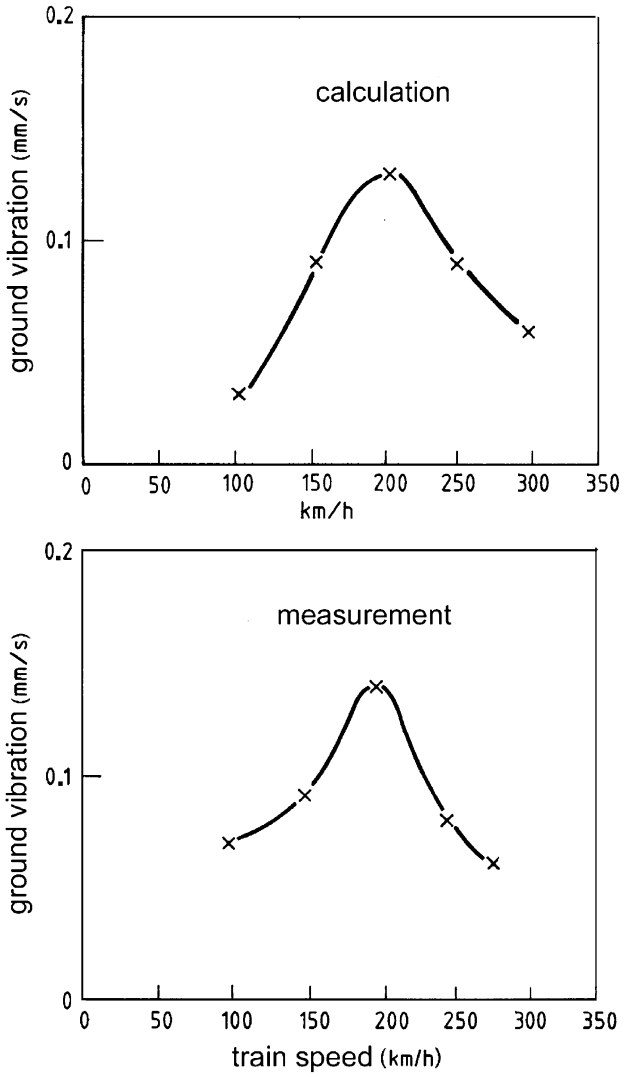

Fig. 12. The sleeper passing part of the ground vibration at a distance of 10–15 m, theory and measurement.

4. Simultaneous measurements of vehicle, track and soil

At the same place some years later, more complex measurements were performed [12]. Vibrations were measured for three different track situations—surface line, bridge and tunnel—and vibrations were measured on the vehicle (15 points, [22]), on the track (8–10 points each) and on the soil (15 points each). The simultaneous measurements of the vehicle gave a better insight into the excitation processes of the ground vibrations near railway lines.

Certainly, no static axle loads can be observed on the vehicle by dynamic measurements. There is a mid-frequency range which is found to be almost identical for all four wheels measured, and

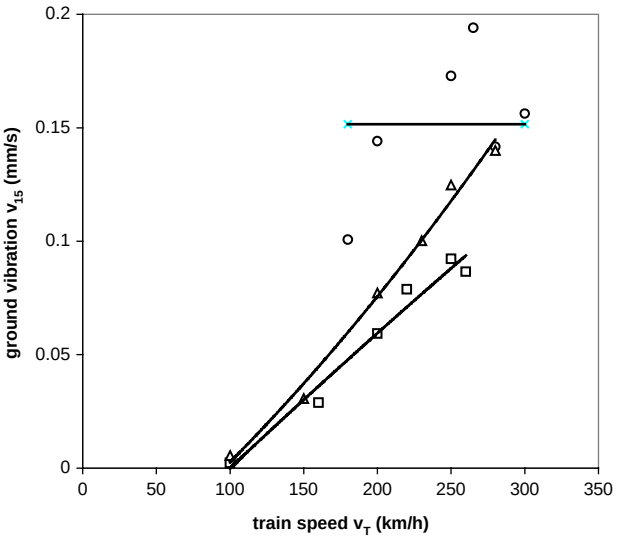

Fig. 13. The mid-frequency part around $f = v_T/2.8\,\mathrm{m}$ of the ground vibration measured during the three test series: 1. 3-unit ICE □, 2. 5-unit ICE ○, 3. 4-unit ICE △.

also identical for all measured speeds of the train, if the frequencies are properly shifted. Therefore, it can be said that these accelerations are due to the *track irregularities*. The track irregularities at this measuring site are approximated by a power law with an exponent higher than 2 (Fig. 16).

The *irregularities of the vehicle* can be found in the Fourier spectra of the accelerations which are given in Fig. 17 for the complete run on the 3 km test section. The unevenness of the wheel is represented by a number of horizontal lines which repeat at the spacing

$$\mathrm{d}f = v_T/2\pi r_W, \tag{35}$$

which is the rotational frequency of the wheel. The amplitudes of these irregularities are between 0.005 and 0.02 mm up to the tenth order $f_{10} = 10\,\mathrm{d}f$.

Now with the excitation known, the calculation as described in Section 2.2 can be performed. The different transfer functions of the ballasted track (Fig. 6) and the slab track (Fig. 7 and Ref. [21]) are multiplied by the irregularities of the track and of the vehicle. The resulting predicted accelerations of the wheelset are given in Fig. 18 together with the ones measured. The correlation between theory and measurement is very good. Both show a clear vehicle–track resonance for the slab track, while for the ballasted track the vehicle–track resonance is at a higher frequency and not so strong as for the slab track with softer pads and lower damping. The differences at lower frequencies are due to the fact that the slab track has a considerably better track quality than a ballasted track [21].

The calculation not only gives the vehicle accelerations but also the dynamic loads on the track, which are almost proportional to the acceleration of the wheel. The response of the surrounding soil can then be calculated in the frequency domain [4]. The spread in frequency due to the Doppler effect is considered approximately. Fig. 19a shows the ground vibration due to the

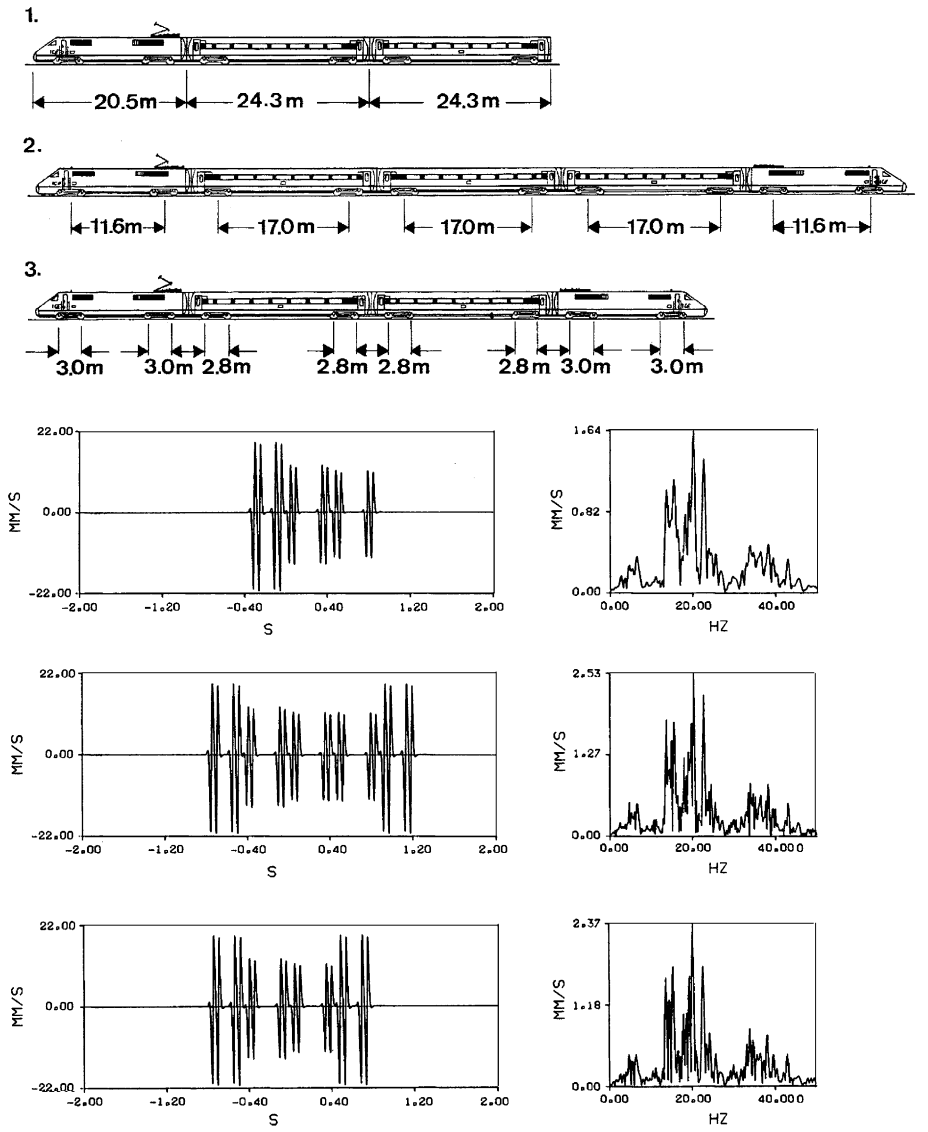

Fig. 14. The different axle sequences of the three test series and the corresponding spectra for $v_T = 200$ km/h.

irregularities of the track, the irregularities of the vehicle and the sleeper-passage excitation. The agreement with the measured ground vibration in Fig. 19b is acceptable, the dependence on the train speed being less pronounced in experiment than in theory. The mid- and the high-frequency part of the vibrations are clearly distinguishable and their amplitudes are nearly the same in theory and experiment. But not all measured amplitudes at around 15 Hz can be represented by the theory. Therefore, a second calculation is presented in Fig. 19c where a scattered part of the axle impulses is added in an approximate manner, giving a better explanation of the mid-frequency amplitudes. From these simultaneous measurements one may conclude again that the

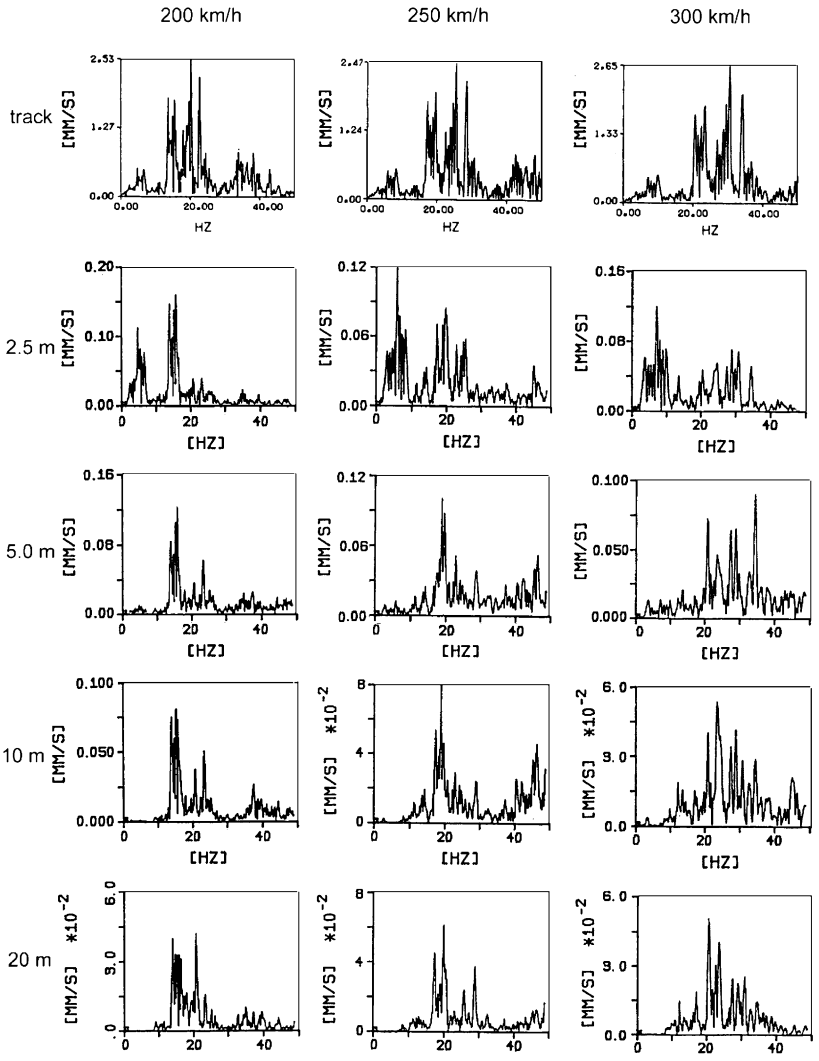

Fig. 15. Spectra of the ground vibration at $r = 2.5$, 5, 10 and 20 m (bottom) compared to the spectrum of the axle sequence (top), three passages of a 5-unit ICE with speeds of 200, 250 and 300 km/h.

scattering of axle impulses is one of the causes of the mid-frequency component of the ground vibrations near railway lines.

5. Conclusion

The passage of the *static axle loads* is important for the track and the close surroundings of the track. However, the corresponding amplitudes decrease very rapidly with distance so that these loads are not important for ground vibrations. This was clearly demonstrated with the ICE test-runs.

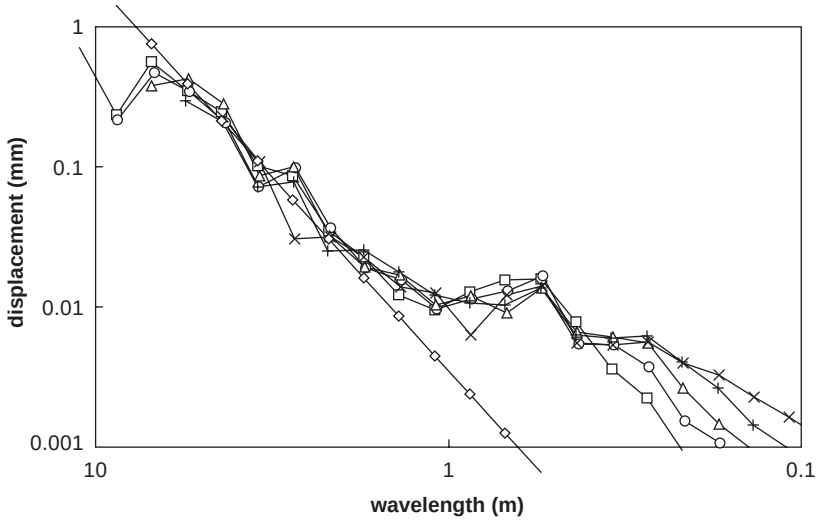

Fig. 16. The *track irregularities* s_T as a function of wavelength, derived from measured vehicle accelerations at the testing site with $v_T = 160$ km/h □, 125 km/h ○, 100 km/h △, 80 km/h +, 63 km/h ×, approximation ◇.

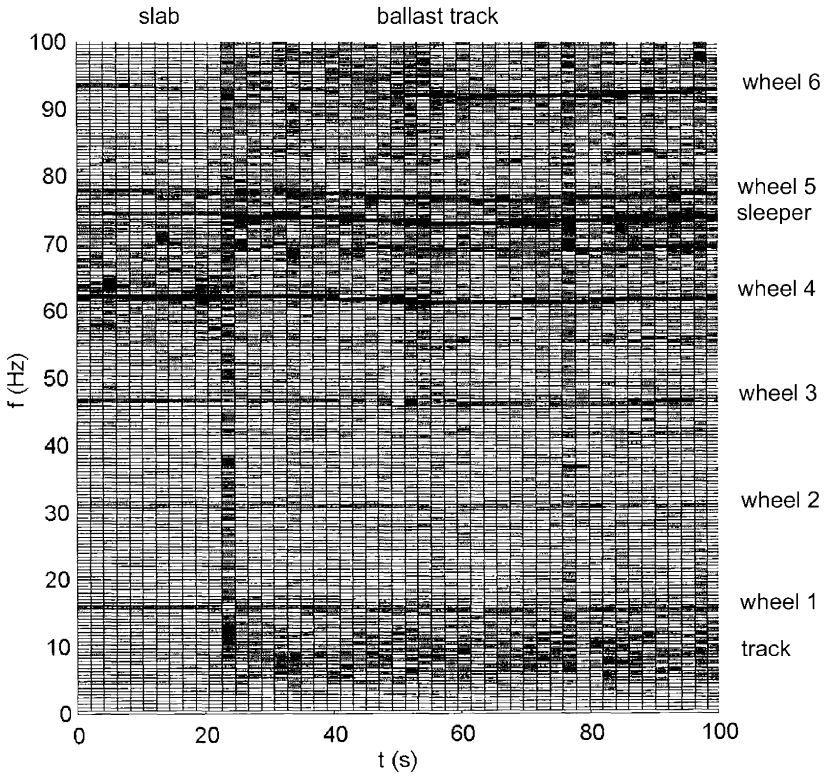

Fig. 17. Fourier spectra of the wheelset accelerations along the complete test section (including ballasted track and slab track, left), indicating the *wheel irregularities*.

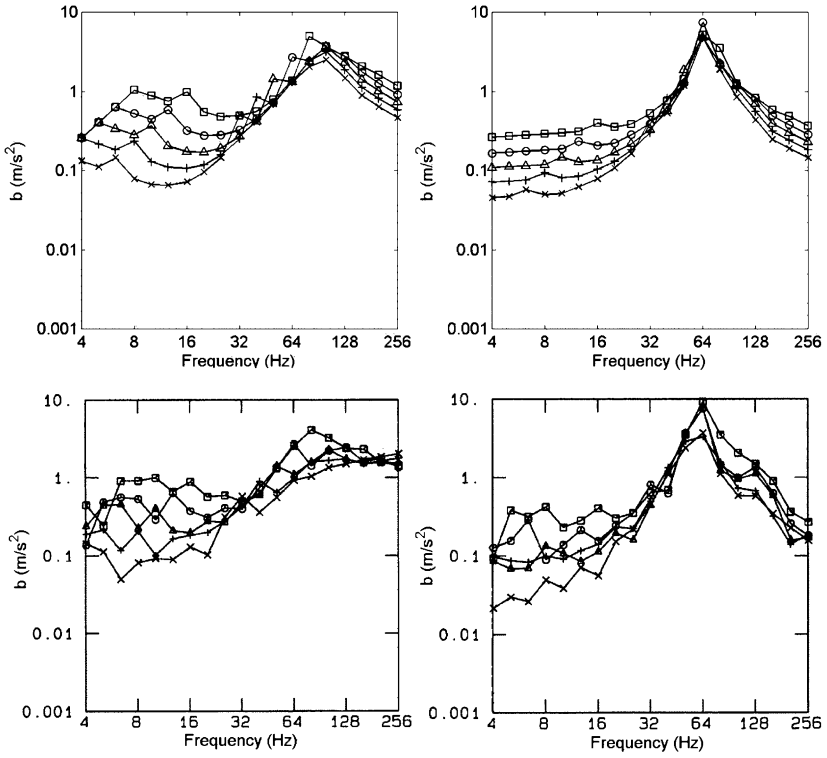

Fig. 18. One-third octave band spectra of the wheelset accelerations at different train speeds $v_T = 160$ km/h □, 125 km/h ○, 100 km/h △, 80 km/h +, 63 km/h ×. Theory (top) and measurement (bottom) of ballasted track (left) and slab track (right).

The effect of *sleeper passage* is well described by the results of parametric excitation presented here. The main effect is a harmonic force which increases with speed but remains constant when the sleeper-passage frequency is higher than the vehicle–track resonance. This was proved by the measurements of the ICE.

The *vehicle–track eigenfrequency* can become more dominant if softer rail pads reduce the radiation damping of the soil as was observed for the slab track measured during the simultaneous measurement.

Irregularities of the vehicle, such as out-of-round wheels, are an important part of the high-frequency excitation as measured under normal conditions. Under test conditions of ICE, this component of excitation was negligible.

Track irregularities can explain the medium-frequency ground vibrations to a certain extent. This was achieved by the simultaneous measurement of the track, the vehicle and the surrounding soil.

From one of the ICE measuring series, the axle-passage impulses were clearly identified in the ground vibrations. This could be explained best by the *scattering of the axle impulses* by a non-uniform soil. Such a stochastic contribution of the passage of static axle-loads would also explain the mid-frequency observations of the simultaneous measurements.

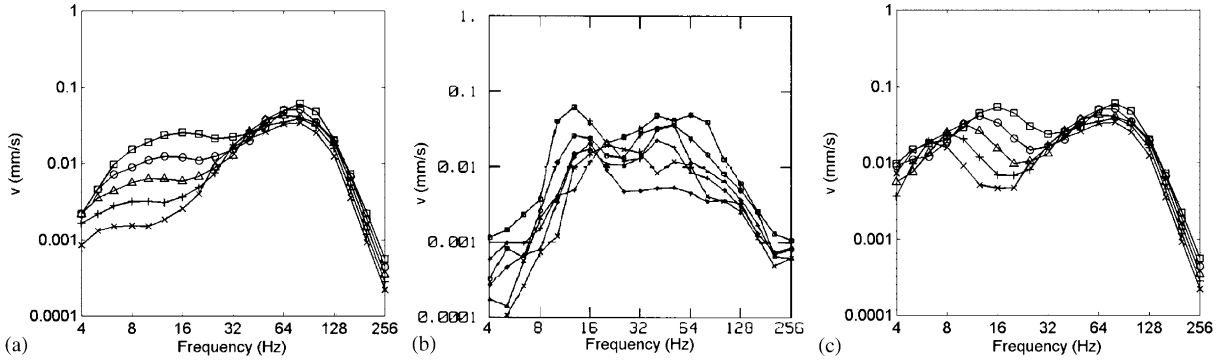

Fig. 19. One-third octave band spectra of the ground vibration at $r = 20$ m and for different train speeds $v_T = 160$ km/h □, 125 km/h ○, 100 km/h △, 80 km/h +, 63 km/h ×. Theory (a), measurement (b) and modified theory (c, with scattering included).

Appendix A. Details of the measured and calculated situations: vehicle, track and soil

Three series with different ICE-*trains* were performed (Fig. 14):

1. locomotive + 2 carriages, $v_T = 100$–260 km/h,
2. locomotive + 3 carriages + locomotive, $v_T = 180$–300 km/h,
3. locomotive + 2 carriages + locomotive, $v_T = 100$–280 km/h,

and the simultaneous measurements were performed with

4. locomotive + 5 carriages + locomotive, $v_T = 16, 25, 40, 63, 80, 100, 125, 140, 160$ km/h.

The static axle loads were

–ICE locomotive and two different carriages, $p_0 = 195$, 130 and 120 kN,
–measuring car (simultaneous measurements), $p_0 = 100$ kN.

The *track* (Fig. 3) consists of a UIC 60 rail with

flexural stiffness $EI = 6.4 \times 10^6\,\mathrm{NM}^2$,
mass per length $\rho A = 60\,\mathrm{kg/m}$,

and stiff rail pads,

concrete sleepers of 2.6 m × 0.26 m × 0.2 m with $d = 0.6$ m sleeper spacing and

$E = 3 \times 10^{10}\,\mathrm{N/m}^2$ modulus elasticity,
$y = 0.15$ the Poisson's ratio,
$\rho = 2.5 \times 10^3\,\mathrm{kg/m}^3$ density,

and, in case of the slab track (simultaneous measurements), an additional concrete plate of 2.6 m × 0.2 m and medium soft rail pads.

The *soil* (as well as the ballast) is represented by the parameters

$\rho = 2 \times 10^3\,\mathrm{kg/m}^3$ mass density,
$v = 0.33$ Poisson's ratio,
$G = 1.5 \times 10^8\,\mathrm{N/m}^2$ shear modulus or
$v_S = 270\,\mathrm{m/s}$ shear-wave speed,
$D = 5\%$ material damping.

Appendix B. The sleeper passage component—a simple approximate solution

Supposing we have a one-dimensional system equation

$$(K + k_1 \sin \omega_S t)u = p_0,$$

where u is the time history of the displacement of the wheel, p_0 the static axle load and K is a dynamic stiffness operator which calculates the time history of the force corresponding to the displacement history u. The simplest example would be

$$Ku = m\ddot{u} + c\dot{u} + ku,$$

with mass m, damping c and stiffness k. We have a corresponding transfer function $K(\omega)$ in frequency domain or for time harmonic forces and displacements. In case of the simple example, the transfer function would be

$$K(\omega) = -m\omega^2 + ci\omega + k.$$

We have a harmonic variation k_1 of the static stiffness with circular frequency ω_S. The amplitude of the stiffness variation is small compared to the dynamic stiffness

$$\left|\frac{k_1}{K(\omega)}\right| < \varepsilon \ll 1.$$

The motivation for these special assumptions is given at the end of this appendix. It is shown that we get the approximate solution of the real situation in railway dynamics.

We find the solution of the time varying problem by two steps. First, we calculate the mean static solution

$$u_0 = \frac{p_0}{K(0)},$$

which fulfils the system equation

$$(K + k_1 \sin \omega_S t)u_0 = p_0 + k_1 \sin \omega_S t u_0$$

with a small error $k_1 \sin \omega_S t u_0$. In a second step, an additional solution

$$u_1 = \frac{k_1 \sin(\omega_S t - \varphi)u_0}{\left|K(\omega_S)\right|}$$

is calculated which compensates for this error

$$Ku_1 = -k_1 \sin \omega_S t\, u_0.$$

The approximate solution

$$u = u_0 + u_1$$

fulfils the time-dependent system equation with a second-order error

$$\begin{aligned}(K + k_1 \sin \omega_S t)(u_0 + u_1) &= Ku_0 + Ku_1 + k_1 \sin \omega_S t\, u_0 + k_1 \sin \omega_S t\, u_1 \\ &= p_0 - k_1 \sin \omega_S t\, u_0 + k_1 \sin \omega_S t\, u_0 + O\left(\varepsilon^2\right) \\ &= p_0 + O\left(\varepsilon^2\right).\end{aligned}$$

The amplitude of the additional displacement due to the variation of the stiffness is

$$u_1(\omega_S) = -\frac{k_1 p_0}{K(\omega_S)K(0)}.$$

and the amplitude of the additional dynamic axle load is

$$p_1(\omega_S) = -\frac{K_V k_1 p_0}{K(\omega_S)K(0)}.$$

The simple method presented in this appendix can be extended to more general variations, for example, to time-dependent mass m_1 and damping c_1, or to higher harmonics of the sleeper passing frequency. But these variations are not of practical importance [20,8].

If we regard a more general load, for example, a harmonic load with frequency f, the response on a track for which the stiffness varies harmonically with frequency f_S becomes

$$Ku_1 = -k_1 \sin\omega_S t u_0 = -k_1 \sin\omega_S t u_0 \sin\omega t = k_1 u_0[\cos(\omega_S + \omega)t + \cos(\omega_S - \omega)t]/2$$

so that u_1 would also include contributions with frequencies

$$f_i = f \pm f_S.$$

But all other load components are small compared to the static load, so that only the static load needs to be included in the time-dependent analysis.

It should be pointed out that it is not necessary to know the system equation explicitly, as only the transfer functions of the vehicle and the track are used and we only need the static value k_1. The latter is a consequence of the general analysis in Section 2.3.1 if restricted to the static load and to the first step of the solution.

Appendix C. The characteristics of spectra due to the passage of a number of axles

First it must be repeated that the spectra due to the passage of static axle-loads are relevant only for the track and its close neighbourhood while for the ground vibration, it is only a possible additional component in case of a non-uniform soil. For these situations, the rules of the very characteristic spectra are stated below.

The passage of a train consists of a number of similar events with certain delay times

$$u(t) = \sum_{i=1}^{n} u_0(t - T_i). \tag{C.1}$$

When this equation is transformed to frequency domain we get for the spectrum of $u(t)$ with the rule for a delay time

$$U(f) = U_0(f) \sum_{i=1}^{n} \mathrm{e}^{-\mathrm{j}2\pi f T_i} =: U_0(f)X(f) \tag{C.2}$$

a product of the spectrum $U_0(f)$ of the single axle and of a spectrum $X(f)$ which characterises the sequence of the axles.

If we look at only two axles (for example of a bogie), the amplitude spectrum is

$$X(f) = 1 + \mathrm{e}^{-\mathrm{j}2\pi fT} \rightarrow \left|X(f)\right| = 2\left|\cos \pi fT\right|. \tag{C.3}$$

This spectrum has maxima at

$$f = 1/T, 2/T, \ldots, n/T, \tag{C.4}$$

which means that the succession of the axles does not prefer a certain frequency region nor are there significant peaks in the spectrum. More characteristically the zeros of the spectrum are at

$$f = 1/2T, 3/2T, \ldots, (2n+1)/2T. \tag{C.5}$$

The zero frequencies remain constant if we have products of sequence spectra, for example a pair of axles, a pair of bogies, a pair of carriages yields

$$X(f) = X_A(f)X_B(f)X_C(f). \tag{C.6}$$

These rules are illustrated by the following figures which are based on the impulse of an axle measured as the particle velocity of the track. The maximum of the spectrum is already determined by the characteristic of the impulse (Fig. 20a). Fig. 20b shows the characteristic zeros and the additional relative maxima. With two bogies (Fig. 20c), we get a number of additional cuts (zeros). For the sequence of a number of carriages in Fig. 21, we get more cuts and with a

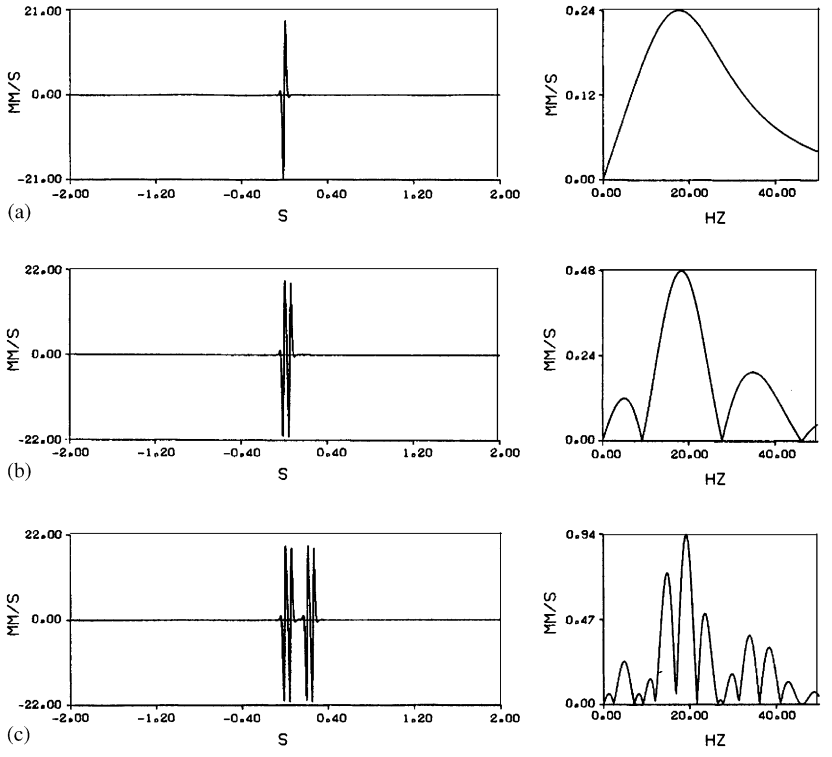

Fig. 20. The axle-sequence spectra of an axle (a), a bogie (b) and a carriage (c), $v_T = 200$ km/h.

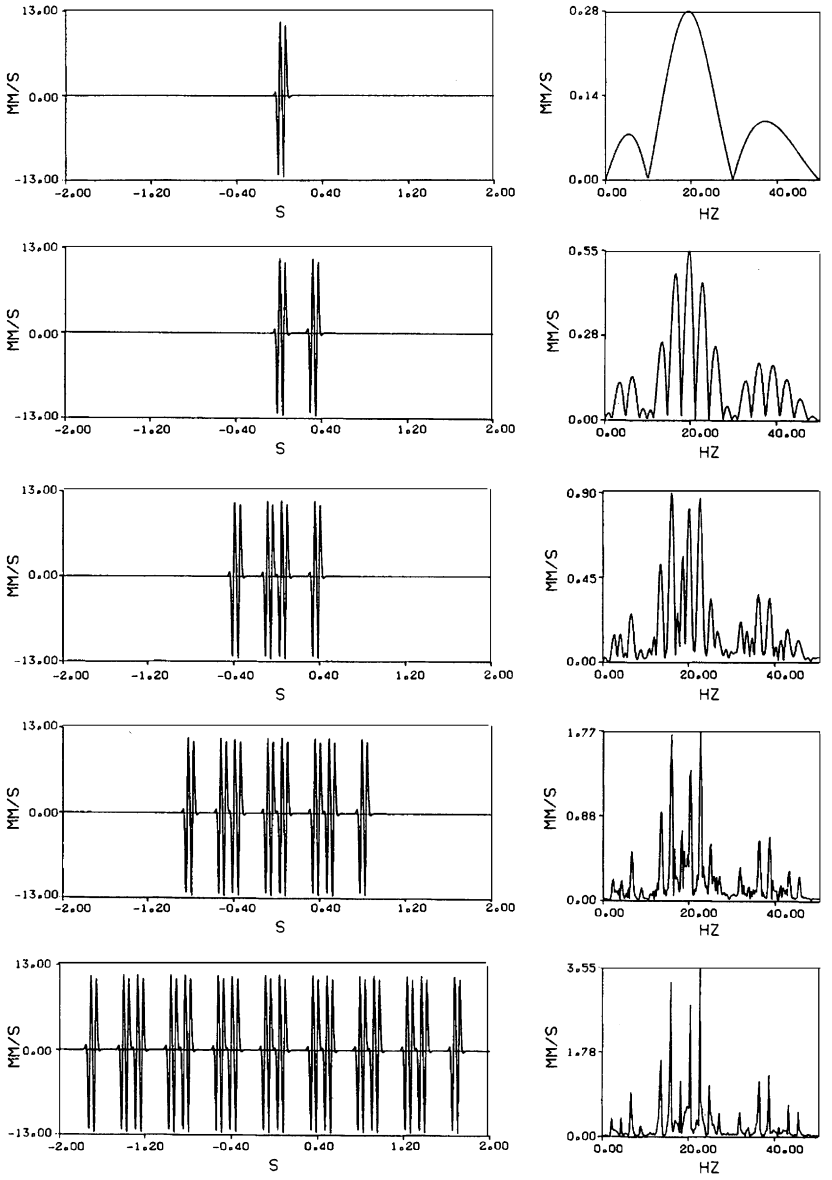

Fig. 21. The axle-sequence spectra of one carriage (top), two, four and eight carriages (bottom), $v_T = 200$ km/h.

high number of similar carriages the maxima get sharper. The spectrum turns into the discrete spectrum of a periodic signal, with a small $\mathrm{d}f = v_T/a_C$ which is ruled by the length a_C of the carriage.

When we look finally at the spectra of the different ICE trains measured (Fig. 14), we find the characteristic cuts at about 10 and 30 Hz and characteristic maxima at 13.5, 15.5, 20, and 23 Hz. The frequencies related to the axle-distance a_A are $\mathrm{f} = v_T/a_A = 18.5$ Hz (locomotive) or 19.8 Hz

(carriage) close to the observed maxima which is due to the fact that the original impulse has its maximum at about 20 Hz. A sharper or a softer impulse would give higher or lower maximum frequencies.

References

[1] T.M. Dawn, C.G. Stanworth, Ground vibrations from passing trains, *Journal of Sound and Vibration* 66 (1979) 355–362.

[2] C.J.C. Jones, J.R. Block, Prediction of ground vibration from freight trains, *Journal of Sound and Vibration* 193 (1996) 205–213.

[3] C. Madshus, A. Kaynia, High speed railway lines on soft ground: dynamic behaviour at critical speed, *Journal of Sound and Vibration* 231 (2000) 689–701.

[4] L. Auersch, Wave propagation in layered soil: theoretical solution in wavenumber domain and experimental results of hammer and railway traffic excitation, *Journal of Sound and Vibration* 173 (1994) 233–264.

[5] R.A.J. Ford, Track and ground vibrations from trains running on conventional ballasted track, *Proceedings of the Institution of Mechanical Engineers, Rail and Rapid Transport* 206 (1992) 117–126.

[6] V. Krylov, Effects of track properties on ground vibrations generated by high-speed trains, *Acustica-Acta Acustica* 84 (1998) 78–90.

[7] L. Auersch, Zur Parametererregung des Rad-Schiene-Systems: Berechnung der Fahrzeug-Fahrweg-Untergrund-Dynamik und experimentelle Verifikation am Hochgeschwindigkeitszug Intercity Experimental, *Ingenieur-Archiv* 60 (1990) 141–156.

[8] A. Nordborg, Vertical Rail Vibrations: Noise and Structure-borne Sound Generation, Doctoral Thesis, KTH Stockholm, 1995.

[9] G. Degrande, G. Lombaert, High-speed train induced free-field vibrations: in situ measurements and numerical modelling, in: N. Chouw, G. Schmid (Eds.), *Proceedings of WAVE 2000*, A.A. Balkema, Rotterdam, 2000, pp. 29–42.

[10] L. Auersch, Zur Entstehung und Ausbreitung von Schienenverkehrserschütterungen: Theoretische Untersuchungen und Messungen am Hochgeschwindigkeitszug Intercity Experimental, BAM-Forschungsbericht 155, Berlin, 1988.

[11] G. Huber, Erschütterungsausbreitung beim Rad/Schiene-System, Dissertation, Universität Karlsruhe, 1988.

[12] L. Auersch, S. Said, W. Rücker, Das Fahrzeug–Fahrweg-Verhalten und die Umgebungserschütterungen bei Eisenbahnen, BAM-Forschungsbericht 243, Berlin, 2001.

[13] X. Sheng, C.J.C. Jones, M. Petyt, Ground vibration generated by a load acting along a railway track, *Journal of Sound and Vibration* 228 (1999) 129–156.

[14] C. Bode, R. Hirschauer, S. Savidis, Three-dimensional time domain analysis of moving loads on railway tracks on layered soils, in: N. Chouw, G. Schmid (Eds.), *Proceedings of WAVE 2000*, A.A. Balkema, Rotterdam, 2000, pp. 3–12.

[15] J. Dinkel, Ein semi-analytisches Verfahren zur dynamischen Berechnung des gekoppelten Systems Fahrzeug–Fahrweg–Untergrund für das Oberbausystem Feste Fahrbahn, Dissertation, TU München, 2000.

[16] G. Pflanz, Numerische Untersuchung der elastischen Wellenausbreitung infolge bewegter Lasten mittels der Randelementmethode im Zeitbereich, Dissertation, Universität Bochum, 2001.

[17] L. Auersch, G. Schmid, A simple boundary element formulation and its application to wavefield excited soil–structure interaction, *Earthquake Engineering and Structural Dynamics* 19 (1990) 931–947.

[18] L. Auersch, Fundamentschwingungen und Wellenausbreitung bei inhomogenen Böden—Beiträge zur Dynamik der Verkehrssysteme, BAM-Forschungsbericht 226, Berlin, 1998.

[19] L. Auersch, Zur praxisorientierten Berechnung der Steifigkeit und Dämpfung von Fundamenten und Fahrwegen, in: G. Niederwanger (Ed.), *Proceedings of D-A-CH Erdbebenwesen und Baudynamik*, Universität Innsbruck, 2001, pp. 225–232.

[20] J. Korb, Parametererregung beim Rad-Schiene-System, VDI-Berichte 381, Düsseldorf, 1980, pp. 99–104.

[21] L. Auersch, Die Fahrzeug-Fahrweg-Untergrund-Wechselwirkung bei der Festen Fahrbahn und beim Schottergleis, *Proceedings of Feste Fahrbahn 02*, IFV-Bahntechnik, Berlin, 2002, pp. 1–19.
[22] H.A. Zakel, L. Willenbrink, Körperschallmessungen an einem Bm 235-Wagen bei der Fahrt auf verschiedenen Oberbauten der Neubaustrecke Fulda–Würzburg, Report to BAM, Deutsche Bahn AG Forschungs- und Technologiezentrum, München, 1997.